This version of the article has been accepted for publication, after peer review (when applicable) and is subject to Springer Nature's AM terms of use, but is not the Version of Record and does not reflect post-acceptance improvements, or any corrections. The Version of Record is available online at: http://dx.doi.org/10.1007/s11837-023-05727-4

Low temperature oxidation kinetics of polymer-embedded ECD copper

Emmanuel Chery and Kristof Croes

*imec, Kapeldreef 75, Leuven, 3001,Belgium.

*Corresponding author(s). E-mail(s): emmanuel.chery@imec.be;
Contributing authors: kristof.croes@imec.be;

Abstract

Low temperature copper oxidation results obtained on a photosensitive polymer-based redistribution layer (RDL) process are presented. Focused ion beam (FIB) cross-sections were performed on 2.5 µm thick copper lines embedded in polymer to monitor the growth kinetics of Cu_2O in air for the temperature range 100–200 °C. Below a transition temperature of 143 ± 7 °C, the oxide growth follows a cubic rate law with an activation energy of 0.71 ± 0.06 eV. At higher temperatures, the oxidation process is diffusion controlled and its kinetics follows a parabolic rate law with an activation energy of 0.36 ± 0.03 eV.

Keywords: Copper, Oxidation, Polymer, Redistribution layer

1 Introduction

Copper is one of the most extensively used metals in the field of micro- and optoelectronics thanks to its good electrical, thermal and optical properties. For example, owing to its low electrical resistivity, copper is still widely used as the main material in highly scaled microelectronics interconnects [1, 2]. Recently, a dual-damascene redistribution layer (RDL) process has been proposed where copper lines are embedded in a photo-sensitive polymer [3]. However, a key reliability concern with copper is its ease to oxidize, even at low temperatures, i.e. below 200 °C [4–6] and while it is generally assumed to be a self limiting process [7–10], some authors found that the oxide layer does not protect from further oxidation [11, 12]. As the critical dimensions keep on

shrinking down with the ever increasing demand for faster and more complex systems [13], high rates of oxidation in the copper lines become a major reliability concern [14]. Understanding the oxidation kinetics in the intermediate to low temperature regions is therefore of primary importance.

The theory of metal oxidation, and in particular copper oxidation, has been extensively reviewed [7, 15–22] but only few studies have focused on low temperature oxidation kinetics [4–6, 15, 19, 23–31]. Consequently, while the growth of thick copper oxide films at high temperatures is generally well understood and assumed to follow the parabolic rate law [7, 21], a consensus has not yet emerged for the kinetics of low temperature oxidation processes. Thus, several growth laws, such as the cubic rate law [15, 29, 32], the direct logarithmic law [19], the linear rate law [4, 24, 25, 30, 31, 33], the inverse logarithmic law [4, 5], the parabolic rate law [27, 29, 34–36] or the nth power law [26] have been reported. As a consequence, different growth laws have been proposed for the same temperature and oxide thickness ranges. This situation is most likely resulting from the variety of parameters impacting the oxidation kinetics such as the temperature, the oxygen partial pressure or the copper properties (thickness, grain size, and texture) [22]. Additionally, as copper spontaneously oxidizes upon air exposure, most of these studies were performed in presence of a native oxide at the start of the experiment resulting in an additional parameter to account for in the determination of a growth law.

Studying the low temperature thermal oxidation kinetics of copper lines embedded in a polymer in presence of a native oxide is therefore of essential interest to assess the reliability of polymer based RDL technologies and is the main topic of this work.

2 Experimental

This study was performed using samples manufactured with a semi-additive approach. A 200 nm thick silicon nitride sheet was deposited on top of a 300 mm silicon wafer. Afterwards, a 30 nm Ti thin film followed by a 100 nm Cu seed layer are deposited by Physical Vapor Deposition (PVD) processes. The Ti layer serves both as adhesion and diffusion barrier layer for the copper. Metal line definition is performed by patterning trenches of various widths in a thick photo-resist using a photo-lithography process. The trenches are subsequently partially filled with a 2.7 µm thick polycrystalline copper film by electrochemical deposition (ECD). After resist strip, the copper seed and Ti barrier layers are removed by wet etching. The patterned copper lines are then coated with 3 µm of photosensitive thermoset phenol-based polymer before a final curing step performed at 200 °C in a vacuum oven.

Copper oxidation was induced in a nitrogen-rich dry air environment using a Thermo Scientific Heraeus UT6060 oven. The oxygen content in the oven during the oxidation process was 2 %. Measurements of the oxide thicknesses was achieved through cross-sections of the partly oxidized copper lines by focused ion beam (FIB) milling using a FEI Helios Dual Beam system. Three

to four cross-sections per condition were performed. Charging issues during the imaging process were avoided by depositing a conductive Pt layer on the samples surface.

3 Results and discussions

A cross-section view of a copper wire encapsulated in polymer is shown in Fig. 1. After several hours of storage at high temperature, a uniform layer is visible around the metal line. Fig. 2 presents a Time-of-Flight Secondary Ion Mass Spectrometry (ToF-SIMS) analysis performed on this layer. After sputtering through the polymer, an oxygen rich copper oxide region is detected, which is most likely the signature of cuprous oxide (Cu_2O) in this temperature range [30, 37]. In Fig. 1, Kirkendall voids resulting from the difference in the diffusion rate of copper atoms in the oxide layer ($\sim 10^{-20}$ $cm^2 \cdot s^{-1}$ at 150 °C) [38, 39] and in the copper layer ($\sim 10^{-25}$ $cm^2 \cdot s^{-1}$ at 150 °C) [40, 41] are visible at the interface copper–oxide. The average oxide thickness is measured on the samples as a function of the stress duration and the temperature and is presented on Fig. 3. Due to the limited number of thickness measurements available for each data point, the error bars are built using the range as a measure of the dispersion. A summary of the stress times, temperatures and resulting oxide thicknesses is available in Table I.

An Arrhenius plot [42] of the oxide thickness as function of $1/k_bT$ for a fixed stress duration of 168 hours is presented in Fig. 4. The extraction of the model parameters was performed with the iminuit library [43] (version 1.5.4 in association with Python 3.8.2). Consequently, the error bars on the oxide thickness are used by the solver in the optimization process. From this plot, two distinct trends are observed with a transition temperature around 143 ± 7 °C. Below the transition, an activation energy of 0.71 ± 0.06 eV is extracted, in good agreement with values generally reported for thin copper films in this range of temperatures [24, 27, 29, 31]. At higher temperatures, the activation energy is reduced to 0.36 ± 0.03 eV, suggesting an oxidation mechanism involving copper diffusion along the grain boundaries. This mechanism is commonly reported with poly-crystalline copper [26, 30, 33, 44–47].

In order to understand further the oxidation mechanism ongoing in both temperature ranges, the oxide growth kinetics was recorded around the transition temperature. The oxide thicknesses measured on the samples stressed at 135 °C and 150 °C have been tested against the different growth kinetics proposed in the literature. The Akaike information criterion with a correction for small sample size is used to assess the quality of the model [48]:

$$\mathrm{AIC}_c = \chi^2 + 2k + \frac{2k(k+1)}{n-k-1} \tag{1}$$

with χ^2, a goodness of fit criterion, n, the number of observations and k, the number of fitted parameters. A trade-off between the goodness of fit and the

Table I Description of the experimental conditions applied on the samples used in this study and resulting oxide thickness measured.

Sample set	Temperature (°C)	Time (hrs)	Oxide thickness (nm)
1	100	168	19.52 ± 5.14
2	110	168	33.10 ± 2.57
3	110	402.25	41.09 ± 5.14
4	125	168	63.34 ± 7.70
5	135	24	40.23 ± 7.70
6	135	48	58.20 ± 9.42
7	135	72	64.20 ± 10.27
8	135	120	102.29 ± 17.14
9	135	168	125.27 ± 8.95
10	135	212	133.53 ± 24.00
11	135	332	157.50 ± 13.70
12	150	30	56.83 ± 14.90
13	150	40.5	70.19 ± 15.41
14	150	48	76.46 ± 17.12
15	150	72	111.25 ± 20.53
16	150	96	142.10 ± 10.25
17	150	120.12	139.23 ± 17.15
18	150	144	156.33 ± 17.95
19	150	168	201.03 ± 30.85
20	150	401	291.68 ± 13.70
21	150	712	387.58 ± 17.10
22	150	1000	482.04 ± 20.55
23	160	168	262.80 ± 17.96
24	175	72	204.27 ± 26.50
25	175	168	332.67 ± 29.10
26	200	168	572.25 ± 14.65

complexity of the model is achieved by minimizing the corrected Akaike information criterion. As shown in Table II, when the oxidation is performed at 150 °C, the AIC_c is minimal for the quadratic kinetics (AIC_c around 8.74) which therefore appears to offer the best fit with a minimal number of parameters. On the other hand, when the oxidation temperature is reduced to 135 °C, the quadratic and cubic growth kinetics are difficult to distinguish based only on the AIC_c (AIC_c around 9.3 to 9.4) and a physics based approach is needed. Using the extracted model parameters, the nucleation time (delay before the growth of the oxide layer begins) can be extracted. At 135 °C, assuming a quadratic law, the onset of oxidation would be observed after 40 minutes whereas at 150 °C, the oxidation process is only detected after 2.6 hours. On the contrary, the cubic kinetics yields a nucleation time above 4.9 hours at 135 °C, strongly suggesting that this growth kinetics should be favored at that temperature. The resulting modelizations are presented in Fig. 5.

These observations are in good agreement with the oxidation theory of Cabrera and Mott [7]. A quadratic rate law is expected for sufficiently high temperatures and sufficiently thick films, when either the metal or the oxygen is soluble in the oxide. The concentration of metal or oxygen at the interface

Table II AIC$_c$ goodness of fit values for the different models reported in the literature and applied on the oxidation results obtained at 150 °C and 135 °C. In the formulae, X is the oxide thickness, t represents the time while A and B are constants.

Model	Formula	AIC$_c$ 150 °C	AIC$_c$ 135 °C
linear	$X = A + B \cdot t$	33.59	14.51
quadratic	$X = A + B \cdot \sqrt{t}$	8.74	9.38
cubic	$X = A + B \cdot \sqrt[3]{t}$	10.58	9.34
quartic	$X = A + B \cdot \sqrt[4]{t}$	14.16	9.67
inverse log	$1/X = A + B \cdot \ln(t)$	25.15	14.83
direct log	$X = A + B \cdot \ln(t)$	36.77	11.95
n$^{\text{th}}$ power	$X = A + B \cdot \sqrt[n]{t}$	12.51[a]	16.25[b]

[a]Solver optimal n = 2.164

[b]Solver optimal n = 2.432

metal–oxide and oxide–air are therefore different and a concentration gradient inversely proportional to the oxide thickness appears. Under the pressure of this gradient, the metal or oxygen diffuses through the oxide layer. The oxide growth rate, dX/dt is thus proportional to 1/X and integration leads to the parabolic rate law $X^2 \sim t$ [7]. On the other hand, in the region of intermediate to low temperatures, a deviation from the quadratic growth is expected due to the presence of a thick space charge layer inside the oxide [15], resulting in a slow down of the diffusion process. At these temperatures, copper is therefore predicted to oxidize according to a cubic law [7]. Recently, a transition between the two laws around 120 to 140 °C was reported [29] in good agreement with the transition temperature of 143 ± 7 °C observed in this study.

By combining the growth laws and the Arrhenius dependency, a general model of the oxide growth kinetics can be expressed as

$$X = \left(A + B \cdot \sqrt[n]{t}\right) \cdot \exp\left(-\frac{E_a}{k_b \cdot T}\right) \tag{2}$$

where X, t, T and n are respectively the oxide thickness, the time, the temperature and the growth law exponent. A, B and E_a are constants, while k_b is the Boltzmann constant. A modelization of the oxide thickness growth using this model is presented in Fig. 6. Temperatures below 143 °C are modeled using n equal to 3 and an activation energy of 0.71 eV. Higher temperatures are described with n equal to 2 and an activation energy of 0.36 eV. A and B constants are extracted using the oxide thicknesses measured at 135 °C and 150 °C for the cubic and quadratic growth law respectively. An excellent agreement between the model and the experimental data is observed confirming the validity of the general model.

4 Conclusions

The oxidation kinetics of polymer-encapsulated copper wires was investigated in the low temperature regime (100—200 °C) in presence of a native oxide. Measurements of the oxide thickness were achieved through cross-sections of the metal lines by FIB milling. Above a transition temperature of 143 ± 7 °C, the oxide growth kinetics is found to follow a quadratic rate law confirming that the oxidation process is diffusion controlled. In this temperature range, an activation energy of 0.36 ± 0.03 eV is extracted. Below the transition temperature, in agreement with the theory of Cabrera and Mott, the growth kinetics is best described by a cubic rate law. At these temperature, the activation energy is 0.71 ± 0.06 eV. As a consequence of these findings, reliability studies of polymer based RDL technologies should be performed below 140 °C to trigger a degradation mechanism coherent with the targeted field applications of this technology.

Acknowledgments. The authors would like to express their gratitude to the different imec teams involved in this study. Contributions from imec's 3D IIAP program are deeply acknowledged. Special thanks for the numerous FIB cross-section requests handled by Dr. E. Vancoille and Dr. Olivier Richard.

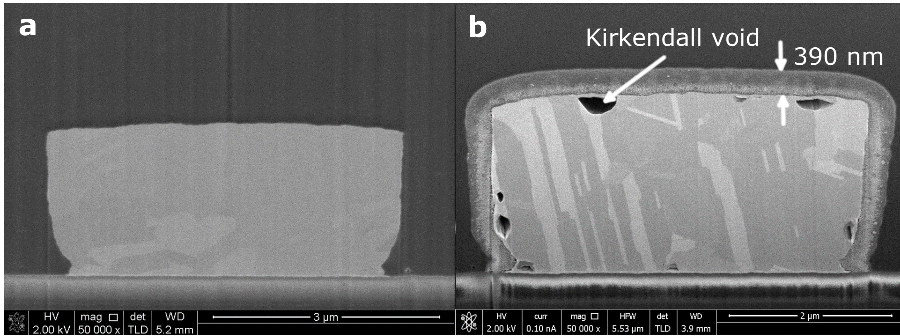

Fig. 1 FIB cross-sections of a copper metal line encapsulated in polymer. a) Reference unstressed sample. b) After 712 hours spent at 150 °C, a 390 nm thick oxide layer is uniformly present around the line and Kirkendall voids appeared at the interface copper–oxide.

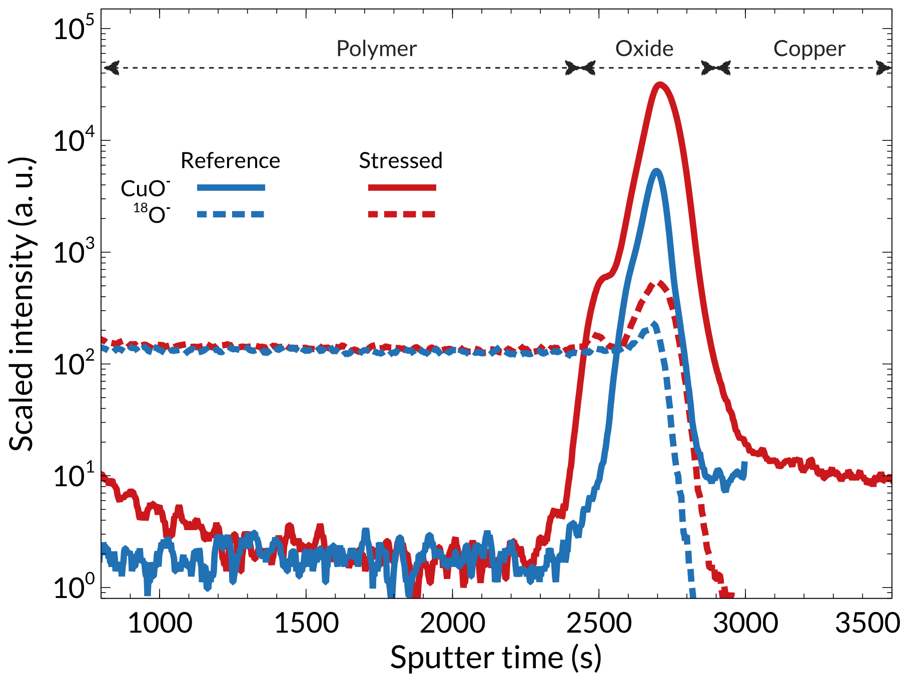

Fig. 2 ToF-SIMS analysis performed on a copper metal line encapsulated in polymer. After 1000 hours at 150 °C, an oxygen rich copper oxide layer is detected on top of the line.

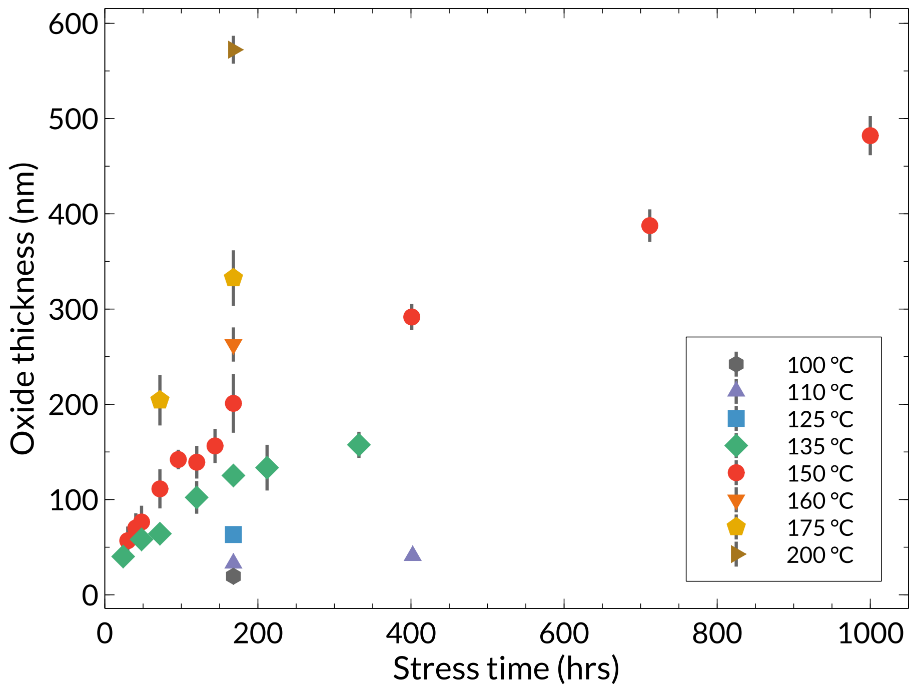

Fig. 3 Oxide thickness measured on top of the copper lines as a function of the stress duration and temperature. The error bars are built using the range as a measure of dispersion.

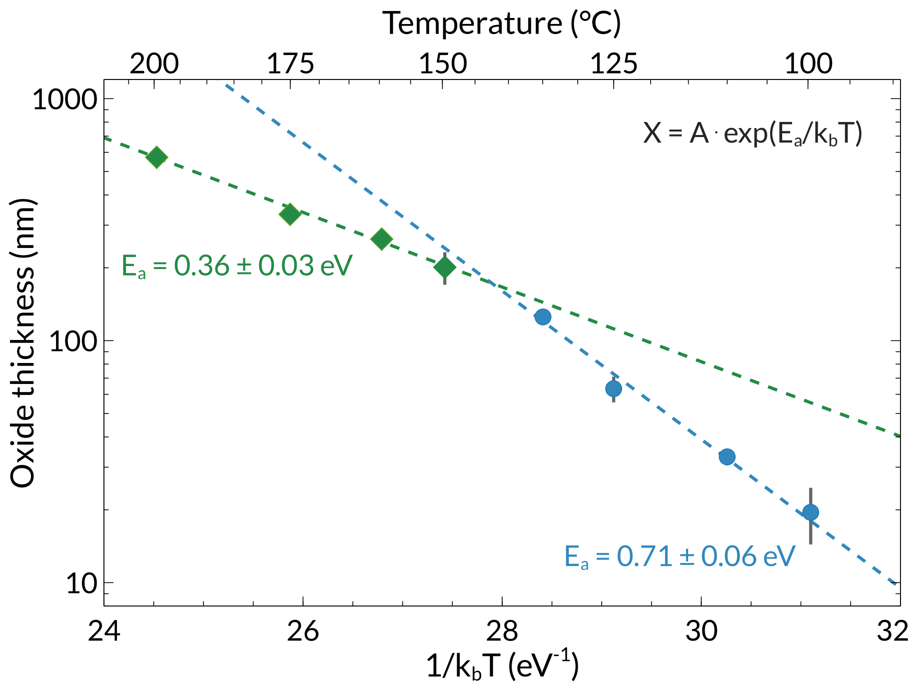

Fig. 4 Arrhenius plot of the oxide thickness as a function of $1/k_bT$ for a fixed stress duration of 168 hours. Two distinct trends are noticed. Below a transition temperature of 143 ± 7 °C, an activation energy of 0.71 ± 0.06 eV is extracted. At higher temperatures, a reduction of the activation energy to 0.36 ± 0.03 eV is observed.

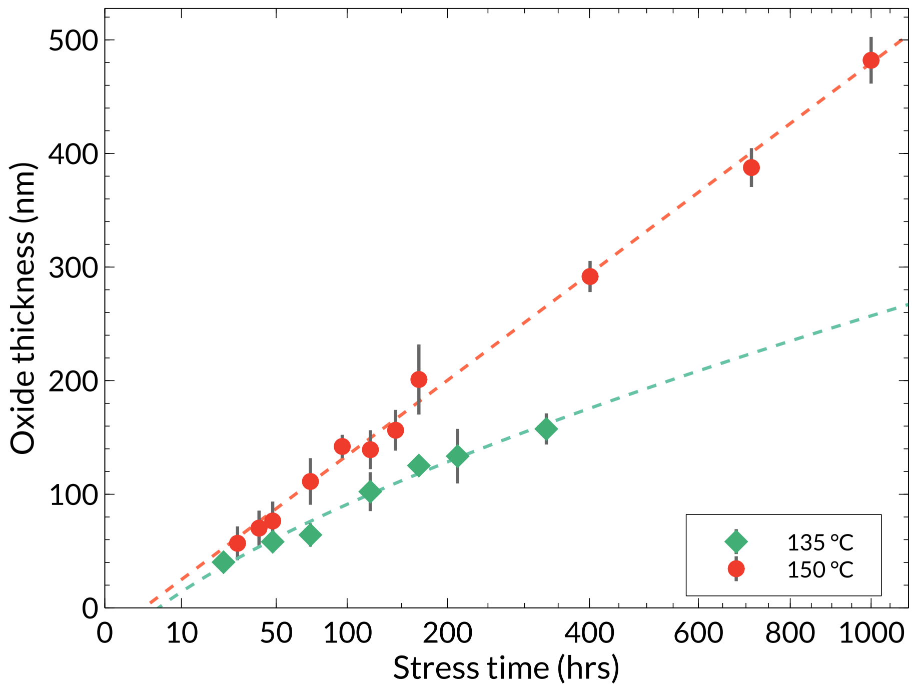

Fig. 5 Oxide thickness as a function of the stress time for samples stressed at 135 °C and 150 °C. The growth kinetics is best described by a cubic law at 135 °C, whereas at 150 °C the quadratic law offers the best fit.

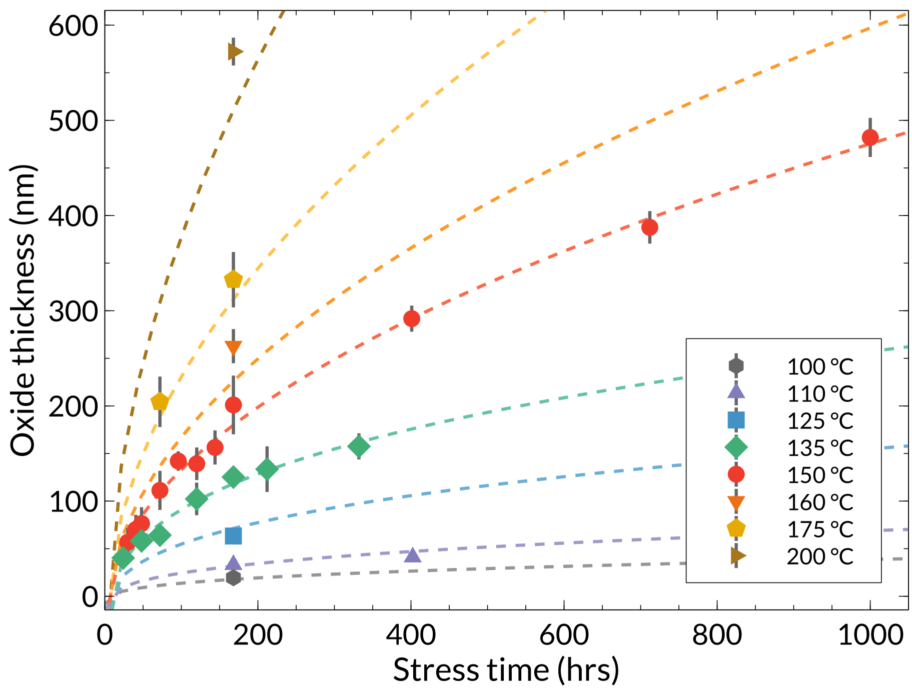

Fig. 6 Oxide thickness growth kinetics as a function of the stress time and temperature. Below 143 °C, data are modeled using n equals to 3 and an activation energy of 0.71 eV. Higher temperatures are described with n equals to 2 and an activation energy of 0.36 eV.

Statements and Declarations

Funding. The authors declare that no funds, grants, or other support were received during the preparation of this manuscript.

Conflict of interest. The authors declare that they have no known competing financial interests or personal relationships that could have appeared to influence the work reported in this paper.

Author contributions. All authors contributed to the study conception and design. All authors commented on early versions of the manuscript. All authors read and approved the final manuscript.

Availability of data and code. The data and source codes that supports the findings of this study are available within the article and in Figshare (https://doi.org/10.6084/m9.figshare.21821730.v1).

References

[1] M. H. van der Veen, N. Jourdan, V. V. Gonzalez, C. J. Wilson, N. Heylen, O. V. Pedreira, H. Struyf, K. Croes, J. Bömmels, and Z. Tokei, Barrier/-liner stacks for scaling the Cu interconnect metallization, in *International Interconnect Technology Conference / Advanced Metallization Conference (IITC/AMC)*, San Jose, 23-26 May 2016.

[2] N. A. Lanzillo, K. Motoyama, H. Huang, R. R. Robison, and T. Spooner, Appl. Phys. Lett. **116**, 164103 (2020).

[3] W. W. Flack, R. Hsieh, H.-A. Nguyen, J. Slabbekoorn, S. Suhard, A. Miller, A. Hiro, and R. Ridremont, One micron damascene redistribution for fan-out wafer level packaging using a photosensitive dielectric material, in *Electronics Packaging Technology Conference (EPTC)*, Singapore, 04-07 December 2018.

[4] M. O'Reilly, X. Jiang, J. T. Beechinor, S. Lynch, C. NíDheasuna, J. C. Patterson, and G. M. Crean, Appl. Surf. Sci. **91**, 152 (1995).

[5] C. Zhong, Y.-M. Jiang, D.-M. Sun, J. Gong, B. Deng, S. Cao, and J. Li, Chin. J. Phys. **47**, 253 (2009).

[6] S. Choudhary, J. V. N. Sarma, S. Pande, S. Ababou-Girard, P. Turban, B. Lepine, and S. Gangopadhyay, AIP Adv. **8**, 055114 (2018).

[7] N. Cabrera and N. F. Mott, Rep. Prog. Phys. **12**, 163 (1949).

[8] J. C. Yang, B. Kolasa, J. M. Gibson, and M. Yeadon, Appl. Phys. Lett. **73**, 2841 (1998).

[9] Y. S. Chu, I. K. Robinson, and A. A. Gewirth, J. Chem. Phys. **110**, 5952 (1999).

[10] H. Lee and J. Yu, J. Electron. Mater. **37**, 1102 (2008).

[11] M. Ronay and P. Nordlander, Phys. Rev. B **35**, 9403 (1987).

[12] S. Suzuki, Y. Ishikawa, M. Isshiki, and Y. Waseda, Mater. Trans., JIM **38**, 1004 (1997).

[13] E. Chery, J. Slabbekoorn, N. Pinho, A. Miller, and E. Beyne, Advances in photosensitive polymer based damascene RDL processes: Toward submicrometer pitches with more metal layers, in *Electronic Components and Technology Conference (ECTC)*, San Diego, 01 June - 04 July 2021.
[14] E. Chery, F. F. C. Duval, M. Stucchi, J. Slabbekoorn, K. Croes, and E. Beyne, Photosensitive polymer reliability for fine pitch RDL applications, in *Electronic Components and Technology Conference (ECTC)*, Orlando, 03-30 June 2020.
[15] W. E. Campbell and U. B. Thomas, Trans. Electrochem. Soc. **91**, 623 (1947).
[16] K. Hauffe, The Mechanism of Oxidation of Metals—Theory, in *Oxidation of Metals*, ed. K. Hauffe (Plenum Press, New York, 1965), p. 79–143.
[17] F. P. Fehlner and N. F. Mott, Oxid. Met. **2**, 59 (1970).
[18] K. R. Lawless, Rep. Prog. Phys. **37**, 231 (1974).
[19] F. P. Fehlner, J. Electrochem. Soc. **131**, 1645 (1984).
[20] A. Atkinson, Rev. Mod. Phys. **57**, 437 (1985).
[21] K. Mimura, J.-W. Lim, M. Isshiki, Y. Zhu, and Q. Jiang, Metall. Mater. Trans. A **37**, 1231 (2006).
[22] C. Gattinoni and A. Michaelides, Surf. Sci. Rep. **70**, 424 (2015).
[23] J. Li, J. W. Mayer, and E. G. Colgan, J. Appl. Phys. **70**, 2820 (1991).
[24] M. Rauh, H.-U. Finzel, and P. Wißmann, Z. Naturforsch., A: Phys. Sci. **54** (1999).
[25] H. Derin and K. Kantarli, Appl. Phys. A **75**, 391 (2002).
[26] A. Njeh, T. Wieder, and H. Fuess, Surf. Interface Anal. **33**, 626 (2002).
[27] G. K. P. Ramanandan, G. Ramakrishnan, and P. C. M. Planken, J. Appl. Phys. **111**, 123517 (2012).
[28] L. D. L. S. Valladares, D. H. Salinas, A. B. Dominguez, D. A. Najarro, S. Khondaker, T. Mitrelias, C. Barnes, J. A. Aguiar, and Y. Majima, Thin Solid Films **520**, 6368 (2012).
[29] K. Fujita, D. Ando, M. Uchikoshi, K. Mimura, and M. Isshiki, Appl. Surf. Sci. **276**, 347 (2013).
[30] Y. Unutulmazsoy, C. Cancellieri, M. Chiodi, S. Siol, L. Lin, and L. P. H. Jeurgens, J. Appl. Phys. **127**, 065101 (2020).
[31] J. Aromaa, M. Kekkonen, M. Mousapour, A. Jokilaakso, and M. Lundström, Corrosion and Materials Degradation **2**, 625 (2021).
[32] T. N. Rhodin, J. Am. Chem. Soc. **72**, 5102 (1950).
[33] W. Gao, H. Gong, J. He, A. Thomas, L. Chan, and S. Li, Mater. Lett. **51**, 78 (2001).
[34] Y. Z. Hu, R. Sharangpani, and S.-P. Tay, J. Vac. Sci. Technol. A **18**, 2527 (2000).
[35] C. Zhong, Y. Jiang, Y. Luo, B. Deng, L. Zhang, and J. Li, Appl. Phys. A **90**, 263 (2008).
[36] S.-K. Lee, H.-C. Hsu, W.-H. Tuan, S.-K. Lee, H.-C. Hsu, and W.-H. Tuan, Mater. Res. (Sao Carlos, Braz.) **19**, 51 (2016).
[37] V. Figueiredo, E. Elangovan, G. Gonçalves, P. Barquinha, L. Pereira,

N. Franco, E. Alves, R. Martins, and E. Fortunato, Appl. Surf. Sci. **254**, 3949 (2008).
[38] W. J. Moore and B. Selikson, J. Chem. Phys. **19**, 1539 (1951).
[39] W. J. Tomlinson and J. Yates, J. Phys. Chem. Solids **38**, 1205 (1977).
[40] A. Kuper, H. Letaw, L. Slifkin, E. Sonder, and C. T. Tomizuka, Phys. Rev. **96**, 1224 (1954).
[41] K. Maier, Phys. Status Solidi A **44**, 567 (1977).
[42] S. Arrhenius, Z. Phys. Chem. **4**, 226 (1889).
[43] H. Dembinski, P. Ongmongkolkul and the iminuit team, *scikit-hep/iminuit*, 2020.
[44] Y. Zhu, K. Mimura, and M. Isshiki, Mater. Trans. **43**, 2173 (2002).
[45] Y. Zhu, K. Mimura, and M. Isshiki, Oxid. Met. **62**, 207 (2004).
[46] K. P. Rice, A. S. Paterson, and M. P. Stoykovich, Part. Part. Syst. Char. **32**, 373 (2015).
[47] B. Maack and N. Nilius, Corros. Sci. **159**, 108112 (2019).
[48] K. P. Burnham and D. R. Anderson, Sociological Methods & Research **33**, 261 (2004).